Review Article

Insights into Anatomical Basis Prescribing Ventilation-Perfusion Distribution in Lung Periphery

Kazuhiro Yamaguchi*[1], Takao Tsuji[1], Kazutetsu Aoshiba[2], Hiroyuki Nakamura[2] and Shinji Abe[1]

[1]Department of Respiratory Medicine, Tokyo Medical University, Japan

[2]Department of Respiratory Medicine, Tokyo Medical University Ibaraki Medical Center, Japan

*Corresponding author: Kazuhiro Yamaguchi, Department of Respiratory Medicine, Tokyo Medical University, 6-7-1 Nishi-Shinjuku, Shinjuku-ku, Tokyo 160-0023, Japan

Abstract

Some crucial problems regarding structural (anatomical) basis on functional parameters describing gas exchange in lung periphery have remained unsolved. Although many definitions for anatomical gas exchange unit (i.e., acinus) have been proposed, there are no authentic study for certifying that anatomically-defined acinus indeed acts as functional gas exchange unit, as well. Among different acini reported so far, we selected acinus of Haefeli-Bleuer (HB acinus) as the most reliable organization. This is simply because microstructures of HB acinus were precisely examined by aid of scanning electron microscopy in addition to light microscopy. Therefore, we first coped with the issue of whether anatomically-defined HB acinus would meet the definition of functional gas exchange unit, i.e., the gas concentration is constant in any region of this organization. We were confronted with an interesting phenomenon that spatial PO_2 gradient exists along the axial direction of HB acinus over inspiration, but it almost disappears over expiration, leading to the conclusion that anatomically-defined HB acinus indeed acts as functional gas exchange unit on expiration but not on inspiration. This fact certainly indicates that functional gas exchange parameters measured on expiration, such as V_A/Q heterogeneity investigated from Multiple Inert Gas Elimination Technique (MIGET), can be considered to reflect microstructural abnormalities at the level of HB acinus. Subsequently, we tried to validate the issue of whether V_A/Q heterogeneities estimated from MIGET would well explain the structural abnormalities in patients with pathologically-and/or radiologically-confirmed lung diseases.

Keywords: Acinus; Anatomical gas exchange unit; Functional gas exchange unit; V_A/Q heterogeneity; Multiple inert gas elimination technique

Abbreviations

V_A: Alveolar or Effective Ventilation, or Alveolar Volume; Q: Pulmonary Capillary Perfusion; V_A/Q: Ventilation-Perfusion Ratio; MIGET: Multiple Inert Gas Elimination Technique; acinus of HB: acinus of Haefeli-Bleuer and Weibel; TB: Terminal Bronchiole; TrB: Transitional Bronchiole; RB: Respiratory Bronchiole; AD: Alveolar Duct; AS: Alveolar Sac; Z: Generation of Airway From Trachea; Z': Generation of Acinar Airway From Transitional Bronchiole; PFT: Pulmonary Function Test; VC: Vital Capacity; FVC: Forced Vital Capacity; FEV_1: Forced Expiratory Volume During One Second; ATI: Air Trapping Index defined as 100.(VC-FVC)/VC; PEF: Peak Expiratory Flow Rate; FEF_{50}: Forced Expiratory Flow Rate at 50% of FVC; TLC: Total Lung Capacity; FRC: Functional Residual Capacity; RV: Residual Volume; PaO_2: PO_2 in Arterial Blood; $AaDO_2$: Alveolar-Arterial PO_2 Difference; $PaCO_2$: PCO_2 in Arterial Blood; D_{LCO}: Pulmonary Diffusing Capacity For Carbon Monoxide (CO); K_{CO}: Krogh Factor for CO defined as D_{LCO}/V_A, where V_A denotes alveolar volume; Hb: Hemoglobin; Pe: Peclet number; d: diameter of airway tube; u: mean convective flow velocity; D: Binary Diffusion Coefficient of Gas; x: axical distance from terminal alveolar sacs; t: time; C: Concentration of Gas; MBNW: Multi-Breath N_2 Washout; DCDI: Diffusion-Convection-Dependent Inhomogeneity; P: Partial Pressure of Gas; P_A: Partial Pressure of Gas in Alveolar Gas Phase; P_C: Partial Pressure of Gas in Pulmonary Capillary; P_V: Partial Pressure of Gas in Mixed Venous Blood; E: Excretion of Gas (P_A/P_V); R: Retention of Gas (P_C/P_V); λ: Blood-Gas Partition Coefficient; SF_6: Sulfur Hexafluoride; L: Objective Variable Minimized with Respect to Fractional Perfusion; q_j: fractional perfusion; v_j: fractional ventilation; R_i: Measured Arterial Gas Concentration Divided by its Mixed Venous Concentration; W_i: Coefficient For Weight of Each Gas; μ: Lagrange Multiplier; ϕ_j: Compartmental Weight of each V_A/Q Unit; S: Smoothing Term; V_D/V_T: Dead Space Ventilation; Q_S/Q_T: Right-to-Left Shunt; MRI: Magnetic Resonance Imaging; ASL: Arterial Spin Labeling; HPV: Hypoxic Pulmonary Vasoconstriction; COPD: Chronic Obstructive Pulmonary Disease; IP: Interstitial Pneumonia; ARDS: Acute Respiratory Distress Syndrome; PE: Pulmonary Embolism; BO: Bronchiolitis Obliterans; PPFE: Pleuroparenchymal Fibroelastosis; HSCT: Hematopoietic Stem Cell Transplantation; HPS: Hepatopulmonary Syndrome; IVL: Intravascular Lymphomatosis; PVOD: Pulmonary Veno-Occlusive Disease; PCH: Pulmonary Capillary Hemangiomatosis; LCH: Langerhans Cell Histiocytosis; LAM: Lymphangioleiomyomatosis; ANCA: Anti-Neutrophil Cytoplasmic Antibodies; PAP: Pulmonary Alveolar Proteinosis; DOE: Dyspnea on Exertion; CT: Computed Tomography; GGO: Ground Glass Opacity; VATS: Video-Assisted Thoracoscopy; 99mTc-MAA: Perfusion Scan using 99mTechnetium (Tc) Labeled Macro-Agglutinated Albumin (MAA); 81mKr: 81mKripton; NO: Nitric Oxide; FeNO: Fractional Concentration of Exhaled NO

Introduction

Among the functional parameters that estimate gas exchange dynamics in the lung periphery, the continuous distribution of ventilation to perfusion (V_A/Q) gives a particularly important information while diagnosing the functional abnormalities in patients with a variety of lung diseases [1,2]. The heterogeneity of V_A/Q distribution is the key mechanism that gives rise to hypoxemia and/or hypercapnia in patients with a variety of lung diseases. It is worth noting that pulmonary physiology, which stresses the heterogeneity of functional properties leading to impaired overall function, is well ahead of other areas of physiology. In other organs, the heterogeneous distribution of functional properties in an organ is well known but little interest has been directed toward the consequences of such functional heterogeneity. As such, the developmental process of pulmonary physiology is unique in comparison with that of other organs [2]. However, there remains the serious problem in pulmonary gas exchange physiology represented by V_A/Q heterogeneity; that is, the endeavors to ensure the relationship between functional heterogeneity and structural lesion do not end successfully [1]. Although the great efforts of elucidating the direct communication (i.e., the establishment of one-to-one relationship) between structural and functional abnormalities in the lung periphery have been made in the era of the 20th century, particularly from the 1950's to the 1980's, it is hard to say that the efforts to unite them in a variety of directions are successfully enough. Furthermore, it is of clinical necessity to have a profound knowledge about the issue of what structural abnormality is detected from the functional V_A/Q heterogeneity while physicians should do a pathophysiological decision-making against a patient with a certain lung disease. In view of these historical facts and clinical requirements, the present review highlights the issue of specifying the structural (anatomical) backgrounds underlying the functional parameter of continuous distribution of V_A/Q that has been used for estimating gas exchange dynamics in the lung periphery. For accomplishing this purpose, the three matters were comprehensively addressed. (1) What is the most appropriate organization serving as the functional gas exchange unit, which is certainly backed by the structural design of the lung periphery? (2) Is the V_A/Q distribution, which is quantified by means of the Multiple Inert Gas Elimination Technique (MIGET), indeed supported by the structural (anatomical) facts? (3) Based on the measurements of continuous distribution of V_A/Q in patients with pathologically- and/or radiologically-confirmed lung diseases, the attempt was made to certify the structure-function relationships in the lungs with various kinds of specific diseases in a precise fashion.

What is the Most Appropriate Organization Serving as Functional Gas Exchange Unit?

Anatomical design for estimating gas transport in conductive airways: From the anatomical standpoint, the lung is divided into two parts. The region with conductive airways (central and peripheral airways) with a dichotomous branching geometry having no alveoli configures the anatomical dead space, through which environmental air is transported to the lung periphery. On the other hand, the region having a tremendous number of alveoli engaging in gas exchange is defined as the acinus. The morphometric data of airway trees can be abstracted into two types of models that extend from the trachea to the terminal alveolar sacs [3-5]. Model A stresses the basic properties
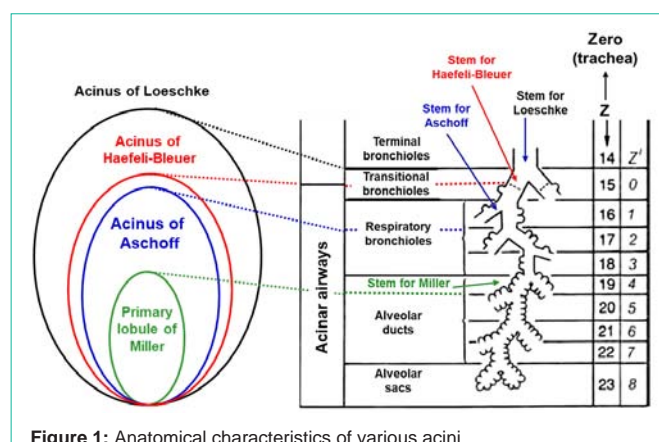

Figure 1: Anatomical characteristics of various acini.
Acinus of Loeschcke is supplied by terminal bronchiole (14th generation). Acinus of Haefeli-Bleuer (HB) and acinus of Aschoff are supplied by transitional bronchiole (15th generation) and first-order respiratory bronchiole (16th generation), respectively. Primary lobule of Miller is served by alveolar duct (19th generation). Z in right panel indicates the number of airway generations from zero (trachea) to 23 (terminal alveolar sac) in model A of Weibel. Z' is the number of airway generations from zero (transitional bronchiole) to 8 (alveolar sacs) in HB acinus. Figure in right side is modified from Reference [5].

of airway branching by assuming the regular dichotomy and thus defining a symmetric typical-path model, while model B defines the irregularities of tree architecture with asymmetric branching and defines the properties of a variable path model.

In the symmetrical typical-path model of A (equivalent to the model A of Weibel [1,5]), the airway branches in a certain generation are assumed to have the same diameter and length. Thus, the diameter-to-length ratio is also treated to be similar in all generations. The total cross-sectional area of all airways in each generation increases tremendously toward the airways located in the periphery. For this feature, the typical-path model of A has been called "trumpet" or "thumbtack" model, as well [6]. In this case, it is necessary to note that the essential factor that defines the airway dimension is the number of generations. The detailed criticisms on the typical-path model of A was found elsewhere [1,5]. Briefly, (1) this model assumes that all anatomical gas exchange units (i.e., acini) are found at an equal distance from the trachea. This is a gross simplification if we gaze the anatomical fact that some terminations of conductive airways end after a shorter distance than others. (2) While the diameter shows a relatively symmetric distribution in airways belonging to the same generation, the segment length is highly skewed. (3) The diameter of acinar airways precisely examined by Haefeli-Bleuer and Weibel [7] is not predicted from the regression line constructed for estimating the diameter of conductive airways.

The starting point for defining the asymmetrical model of B is based on the anatomical finding that airways with a certain diameter occur in several generations and at different distances from the origin of airways [5]. For instance, airways of 2 mm diameter are found in generations 4 to 14, with a maximum in generation 8. Alternatively, these bronchi are located at 18 to 31 cm from the origin of trachea with a maximum at 24 cm. Note that in the symmetrical typical-path model of A, bronchi with 2 mm diameter are located maximally in generation 8 corresponding to 23.6 cm from the trachea, which is in a close agreement with the distance that shows the maximum
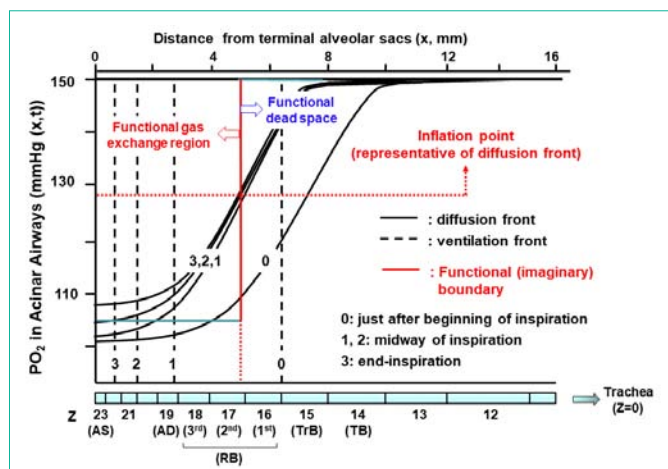
Figure 2: Temporal and spatial PO_2 profiles in HB acinus during inspiration. Theoretical calculations were done based on geometrical data of HB acinus (Table 1). Various conditions for theoretical calculations are the same as taken by ref. 23 except for PO_2 transfer through alveolocapillary membrane. For simplicity, O_2 is assumed to be not absorbed through alveolocapillary membrane in our calculations. Calculations were done under conditions of room air breathing, resting condition, tidal volume of 500 mL, FRC of 3,000 mL, and one respiratory cycle of 5 sec (inspiration: 2.5 sec and expiration: 2.5 sec). We used equations demonstrated by ref. 37, in which convection, axial diffusion, influence of acinar structures on gas mixing, and transitional change of alveolar cross-sectional area during respiration are taken into consideration. To know representative point of diffusion front at a certain time, we calculated inflation point solving equation of $\partial^2 C/\partial x^2 = 0$ under steady state condition ($\partial C/\partial t = 0$). Inflation point gives functional (imaginary) boundary between dead space and alveolar gas exchange region. TB: Terminal Bronchiole; TrB: Transitional Bronchiole; RB: Respiratory Bronchiole; AD: Alveolar Duct; AS: Alveolar Sac.
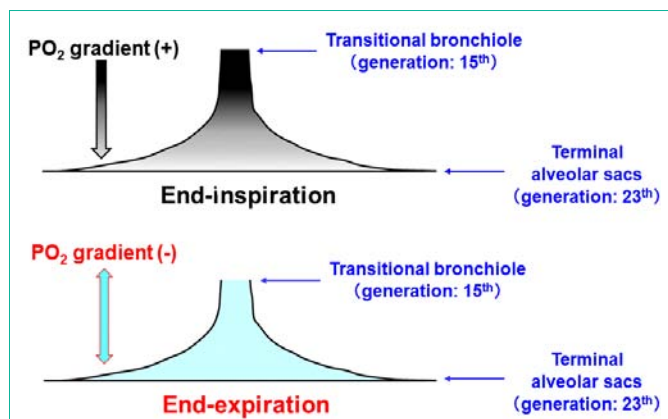

Figure 3: Spatial distribution of PO_2 at end-inspiration and at end-expiration. Temporal and spatial PO_2 profiles shown in (Figure 2) identified that substantial stratified inhomogeneity of PO_2 along axial distance from transitional bronchiole (acinar entrance) to terminal alveolar sacs exists at end-inspiration (upper panel). However, stratification of PO_2 is almost fully eliminated at end-expiration (lower panel).

distribution of bronchi having 2 mm diameter in the variable path model of B [5]. Based on these facts, one may conceive that although the symmetrical typical-path model of A has various limitations, it works approximately as an acceptable model for predicting airway branching, at least in lower conductive airways from trachea to terminal bronchioles. When attempting to precisely evaluate the convection-related gas transport dynamics in conductive airways

toward terminal bronchioles, a more realistic model such as variable path model of B with an asymmetrical branching architecture should be applied. However, when considering the gas mixing dynamics in the acinar region, the difference in models for conductive airways may exert little impact. This is because the relative contribution of diffusion is equivalent to, or predominates, that of convective flow in the acinar region [6].

Anatomical design for estimating gas exchange in lung periphery: The alveolus cannot be taken as a ventilation unit mostly because each alveolus is not independent of other alveoli. Two adjoining alveoli share the alveolar wall and each alveolus adjoins several alveoli, some of which are connected to different alveolar ducts. Furthermore, there are communications at the level of respiratory bronchioles or alveolar ducts defined as Martin channels [8]. In addition, there is a serious problem concerning a perfusion unit formed by the pulmonary microcirculation. The dense, intertwined capillary network embedded in the alveolar wall forms a continuum of blood flow that is not partitioned into independent perfusion units, resulting in that the story one likes to present, i.e., the anatomical gas exchange unit is organized into an alveolus associated with a separated capillary network in the alveolar wall, is highly fictitious. The capillary network is supplied by the arteriole penetrating the acinus along acinar airways and is drained into the venule in the acinar periphery. The distance between an arteriole and a venule is of an order between 0.5 and 1.0 mm [9], resulting in that the perfusion unit given by the area surrounded by an arteriole and a venule extends over several alveoli. These facts are in accord with the idea that the perfusion unit is not congruent with the ventilation unit if it is composed of an alveolus, giving rise to difficulty in anatomically defining the gas exchange unit from an alveolus and a capillary network, in which the ventilation and perfusion units should be matched.

The traditional rationale for anatomical ventilation unit was evolved based on the concept of acinus, the ventilation into which is supplied by a terminal bronchiole (corresponding to the 14th generation in typical-path model of A) that is the last peripheral airway without alveoli. This type of ventilation unit is generally called the acinus of Loeschcke (Figure 1). There are many other terms that define the region equivalent to the acinus of Loeschcke [10-16]. The size of acinus of Loeschcke averages 7 to 10 mm in diameter and roughly 30,000 acini configure the lung. An acinus contains alveoli ranging from 3,000 to 4,000 [7], resulting in that the lung consists of about a hundred million alveoli.

Miller [17] proposed the different anatomical concept that is precious for understanding what the secondary and primary lobules are. The secondary lobule of Miller is the area supplied by a lobular bronchiole having dimeter of about 1.0 mm (corresponding to the 12th generation) and surrounded by the fibrous connective tissue septa (i.e., the interlobular septa). The size of secondary lobule of Miller varies from 1.0 to 2.5 cm, each of which is comprised of varying number of acini defined by Loeschcke, ranging from three to 24 depending on the region selected [10,18], while the primary lobule of Miller is expressed by the area governed by an alveolar duct (corresponding to the 19th generation). However, it may be a mistake to take the primary lobule of Miller as the ventilation unit constituting the anatomical gas exchange unit. This is because there
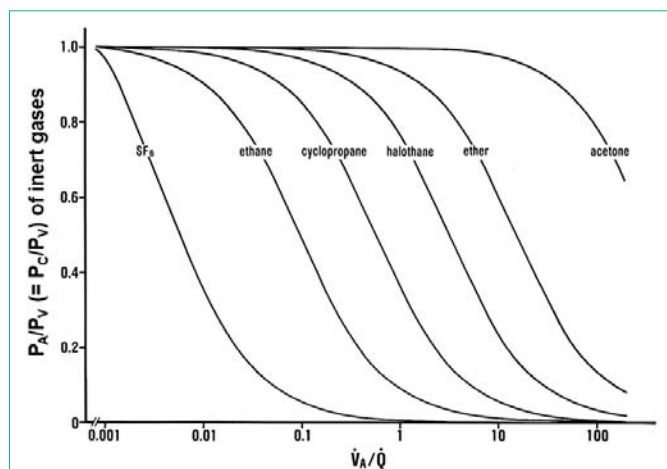
Figure 4: Relationships between blood-gas partition coefficients (λ) of inert gases and $\dot{V}_A/\dot{Q}$ values.
Ordinate: excretion (E = P_A/P_V) or retention (R = P_C/P_V) of inert gases. Abscissa: logarithmic $\dot{V}_A/\dot{Q}$ value. E or R of each inert gas sharply changes in a certain range of $\dot{V}_A/\dot{Q}$ depending on λ. Sharp change in SF_6 is found at $\dot{V}_A/\dot{Q}$ ranging between 0.001 and 0.01. As such, SF_6 has high sensitivity to detecting gas exchange units with very low $\dot{V}_A/\dot{Q}$ values. On the contrary, acetone sharply changes at $\dot{V}_A/\dot{Q}$ ranging from 10 to 100, indicating that acetone is susceptible to gas exchange units with very high $\dot{V}_A/\dot{Q}$ values.
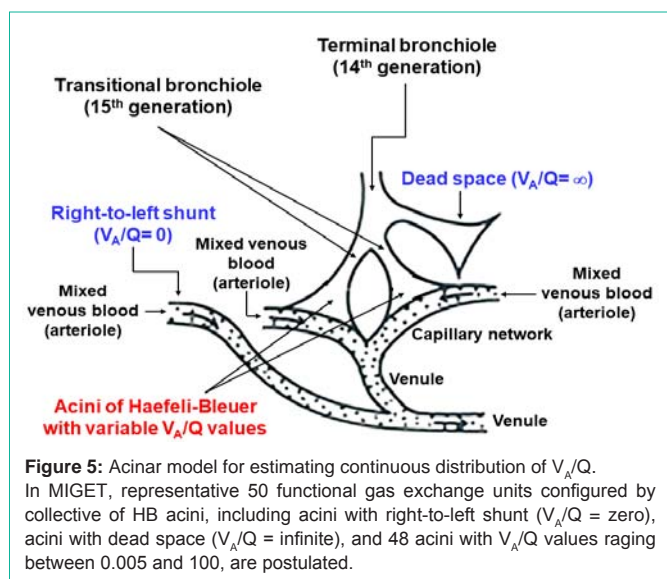

Figure 5: Acinar model for estimating continuous distribution of $\dot{V}_A/\dot{Q}$.
In MIGET, representative 50 functional gas exchange units configured by collective of HB acini, including acini with right-to-left shunt ($\dot{V}_A/\dot{Q}$ = zero), acini with dead space ($\dot{V}_A/\dot{Q}$ = infinite), and 48 acini with $\dot{V}_A/\dot{Q}$ values raging between 0.005 and 100, are postulated.

Table 1: Microstructural characteristics of HB acinus.

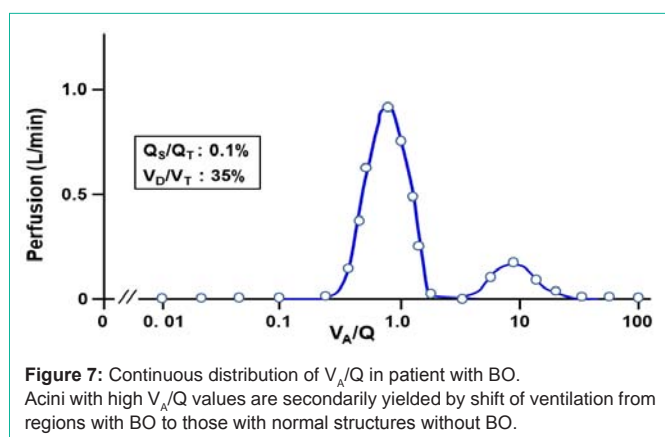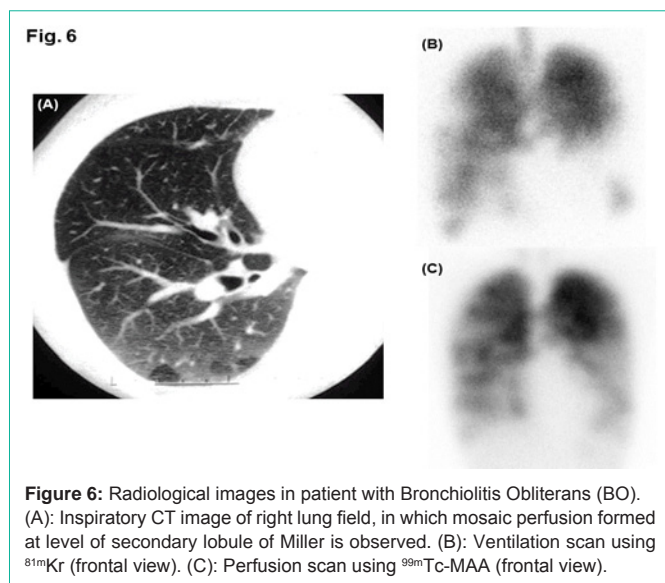| Structural parameters	Comments
Entrance	Transitional Bronchiole (TrB)
Airway branching pattern	Irregular, asymmetrical dichotomy (trichotomy: rare)
Number of branches (Z') Transitional bronchiole: Z' = zero	Average: 9.1 (ranging from 6 to 12)
Total longitudinal path length	8.8 ± 1.4 mm (from TrB to terminal alveolar sacs)
Internal airway diameter	Decrease from 500 μm (Z' = 0) to 270 μm (Z' = 10)
Outer airway diameter	Approximately constant over acinar airways including alveolar sleeve (700 μm)
Total surface area of alveoli	Average: 69 cm^2
Total volume of an acinus	187 ± 79 mm^3
Total number of acini in human lung	26,000 to 32,000

Values are measured under condition at full expansion of lung tissue specimen. Data are extracted from those reported in ref. 7.

Table 2: Blood-gas partition coefficients (λ) of six inert gases used for MIGET.

Species of inert gases	λ (mL/mL at 37°C)
(1) Sulfur hexafluoride (SF_6)	0.009
(2) Ethane	0.091
(3) Cyclopropane	0.583
(4) Halothane	2.82
(5) Diethyl ether	14.4
(6) Acetone	304

was made by Haefeli-Bleuer and Weibel [7], who defined the acinus as the region severed by the proximal part of a transitional bronchiole without identifiable alveoli (the 15th generation). The authors [7] showed that the transitional bronchiole contains the segments both with and without alveoli. We shall name this type of acinus "the acinus of HB" in the present review, which may be larger than the acinus of Aschoff but is smaller than the acinus of Loeschcke. However, as it is extremely difficult to surely separate the transitional bronchiole from the first-order respiratory bronchiole in a microscopic examination [7], there is a certain possibility that the acinus of HB is practically the same as that of Aschoff. Therefore, when the term of the acinus of HB is used in the present review, it also includes the acinus of Aschoff.

The difficult problem concerning the anatomical unit for perfusion was resolved by König et al. [22], who demonstrated that the entire region of Loeschcke is perfused almost homogeneously by a plasma tracer, indicating that all capillary networks existing in the acinus of Loeschcke are connected to each other. Since the acinus of HB is smaller than that of Loeschcke, the fact identified by König et al. [22] holds true for the acinus of HB, as well. Therefore, we addressed the acinus of HB as the most appropriate anatomical gas exchange organization (Table 1). The acinar airways of HB are characterized by asymmetrical, irregular dichotomy (rarely, trichotomy), which branch over 9 generations. The internal airway dimeter falls as the branching progresses, while the outer diameter, including the sleeve of alveoli, remains almost constant. The total path length from the transitional bronchiole to the terminal alveolar sac averages 8.8 mm, while the total acinar volume averages 0.2 cm^3. The total alveolar surface area participating in gas exchange reaches about 70 cm^2.

are many alveoli that are not included in the primary lobule of Miller.

Reid [19,20] proposed a different definition about the secondary lobule. The secondary lobule of Reid is the region distal to any bronchiole with a mm-branching pattern. The size of the secondary lobule of Reid is constant (approximately 1.0 cm) in comparison with that of Miller and contains three to five acini of Loeschcke. The Reid's secondary lobule is useful when interpreting the bronchogram but not evaluating the gas exchange in the lung periphery.

The acinus of Aschoff is defined as the ventilation unit supplied by the first-order respiratory bronchiole (the 16th generation), the size of which is about half of the acinus of Loeschcke [21].

The extensive analysis on the microscopic structure of the acinus

Figure 6: Radiological images in patient with Bronchiolitis Obliterans (BO). (A): Inspiratory CT image of right lung field, in which mosaic perfusion formed at level of secondary lobule of Miller is observed. (B): Ventilation scan using ^{81m}Kr (frontal view). (C): Perfusion scan using ^{99m}Tc-MAA (frontal view).

Figure 7: Continuous distribution of V_A/Q in patient with BO. Acini with high V_A/Q values are secondarily yielded by shift of ventilation from regions with BO to those with normal structures without BO.

However, it should be noticed that these values are measured at an almost full expansion of the lung tissue specimens, corresponding to a Total Lung Capacity (TLC) level. Therefore, under physiological condition, i.e., at a Functional Residual Capacity (FRC) level, the dimensions of acinar structures, including acinar volume and total alveolar surface area, should be considered about half of the values depicted in (Table 1) [23].

Collateral ventilation in the acinus: Three pathways provide the collateral ventilation in the acinus, i.e. alveolar pores (pores of Kohn), channels of Lambert, and channels of Martin. Although the size of alveolar pores ranges from 2 to 30 μm, there are many studies certifying that the alveolar pores are not potent in air-filled lungs [24,25]. These studies indicate that the alveolar pores take no part in maintaining alveolar ventilation.

Lambert [26] described accessory communications between bronchioles and alveoli in the normal human lung. The diameter of Lambert channels varies from zero to 30 μm, and they are considered to serve as collateral ventilation to adjacent alveoli when airway obstruction occurs at the level of terminal bronchioles [25]. Supporting this consideration, the important role of Lambert channels was identified in patients with pneumoconiosis, in which

a striking accumulation of macrophages was found in the Lambert channels and their adjacent alveoli [27].

Martin [8] reported intra-acinar communications at the level of respiratory bronchioles or alveolar ducts in the canine lung. The Martin channels were also found in human lungs [13,28]. As the Martin channels have sufficiently low resistance to gas flow, they act as the primary pathway for inducing collateral ventilation in the acinus [25]. Therefore, one can conceive that only the Martin channels but neither the alveolar pores nor the Lambert channels serve to equalize the acinar ventilation.

Anatomical and functional boundaries between dead space and alveolar region: The anatomical boundary between dead space and alveolar region is very simple, lying at the level of terminal bronchiole having no alveoli, corresponding to the entrance of acinus of Loeschcke. Namely, the dead space is anatomically conceptualized as the space configured by upper and lower conductive airways up to terminal bronchioles [29]. The anatomically-determined dead space volume varies from 140 to 260 mL depending on the extent of lung inflation and age [30-32]. The anatomical studies consistently showed that 50% of the dead space exists in extrathoracic upper airways, indicating that the volume of lower conductive airways, including central and peripheral airways up to terminal bronchioles, ranges between 70 and 130 mL.

The functional boundary between dead space and alveolar region has been examined by many investigators based on single-breath measurements using CO_2, N_2, and foreign inert gases [33-36]. The functional boundary may be better understood to use the term of "imaginary boundary". The results obtained therefrom are comparable to those reported for the anatomical dead space. In this case, the following fact should be recognized, i.e., in addition to the convective transport by ventilation, the contribution of diffusion to overall gas transport rises substantially in acinar regions. The respective importance of convection and diffusion for gas transport in a certain part of the lung can be appreciated from the Peclet number (Pe) as;

$$Pe = d \cdot (u/D) \cdots\cdots \text{Equation 1}$$

where d is diameter of an airway tube, u is convective flow velocity, and D is binary diffusion coefficient of a gas. When the Pe number reaches 1.0, the diffusive transport is the same order of magnitude as the convective transport [37]. Under resting condition with air breathing, the convective flow velocity at the trachea is about 100 cm/sec while about 1 cm/sec at the acinar entrance, indicating that the convective flow velocity falls 100-fold from the trachea to the acinar airways and the contribution of diffusion to gas transport significantly surpasses that of convection within the acinus [5,37]. The position where the Pe is equal to 1.0 is called the critical zone originally proposed by Gomez [38]. The most informative study aiming at specifying the essential mechanism forming the functional boundary between dead space and alveolar region was expanded by Paiva [39]. Incorporating convection, diffusion, and their interaction into the basic mechanism for gas mixing in airways below the 13th generation of symmetrical typical-path model of A (i.e., corresponding closely to the secondary lobule of Miller) [6,40-44], Paiva [39] found that on inspiration, the front of a gas (alternatively called diffusion front), which is the

concentration profile of a gas having the sigmoid shape against the axial distance from the terminal position of the acinus, lags far behind the front of tidal volume. The font of tidal volume reaches the 22th generation of airways (i.e., the alveolar duct) at end-inspiration, whereas the diffusion front remains almost stationary in the second-order respiratory bronchiole during inspiration except for the time point just after beginning of inspiration. The relatively stationary diffusion front indicates that during inspiration, the convective advancement of a gas into the periphery is counterbalanced by the diffusion-elicited proximal retreat of a gas in the acinus [1,6,39]. Qualitatively the similar results were obtained by Swan and Tawhai [23], who applied the asymmetrical branching model of acinar airways (i.e., the acinus of HB) for theoretical analysis. We also estimated the time- and axial distance-dependent PO_2 profiles in an acinus of HB during inspiration and expiration under resting condition with air breathing. We obtained qualitatively the same results as those reported by Swan and Tawhai [23] (Figure 2). These findings suggest that the dead space can be functionally described as the inspiratory volume decided by the diffusion front, but not by the front of tidal volume. The classical gas exchange theory assumes that the dead space has a sharp, all-or-nothing transition boundary as if it is formed only by the ventilation-elicited convection (i.e., the effective ventilation). The effective ventilation may be decided by converting the effect of diffusion to the equivalent effect of convection. The location of effective ventilation is intuitively appreciated by drawing the straight line along the vertical axis, which crosses the representative point of diffusion front. The representative point of diffusion front is given by the inflation point of the sigmoid concentration profile of a gas, which is characterized by the maximal concentration gradient for an intended gas. The inflation point of the symmetrical sigmoid curve is approximated by the point corresponding to the midpoint of the total change in the concentration of a gas generated between acinar entrance and terminal alveolar sacs. When simplifying the complicated results shown in (Figure 2) by considering the effective ventilation point, the functional (imaginary) boundary between dead space and alveolar gas exchange region lies in the second-order respiratory bronchiole, which is distal to the terminal bronchiole and close to the entrance of acinus of HB. This fact suggests that the acinus of HB might also serve as the gas exchange unit in a functional sense.

The Most Appropriate Organization Serving as Functional Gas Exchange Unit: The absolute condition that should be met while defining the functional gas exchange unit is the homogeneous distribution of a gas over the region that forms the unit. The important message derived from the study of Paiva [39] and that of Swan and Tawhai [23] is that a series, stratified inhomogeneity of a gas concentration along acinar airways from entrance to terminal alveolar sacs exists during inspiration, resulting in that regardless of the type of acinus, the anatomically-defined acinus does not satisfy the absolute condition indispensable for establishing the functional gas exchange unit during inspiration. However, the situation is clearly different during expiration. A couple of groups of investigators [23,39,45] demonstrated that the inspiration-elicited stratified inhomogeneity for a gas diminishes rapidly during expiration. Swan and Tawhai [23] identified that the spatial variation of PO_2 in the acinus of HB under resting condition at air breathing is only 3% during expiration, which is qualitatively coincided with our analytical results (Figure 3). Furthermore, the Martin channels,
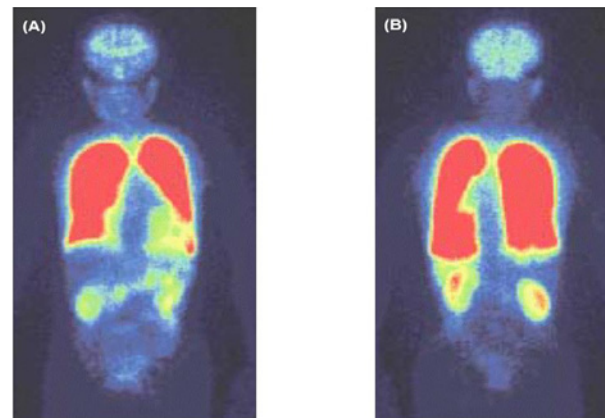

Figure 8: Perfusion scan using [99mTc]-MAA in patient with Hepatopulmonary Syndrome (HPS)
(A): anterior-posterior view, (B): posterior-anterior view. [99mTc]-MAA particles flow into systemic organs, including brain and abdominal organs, indicating significant formation of right-to-left shunt, which amounts to 28%.
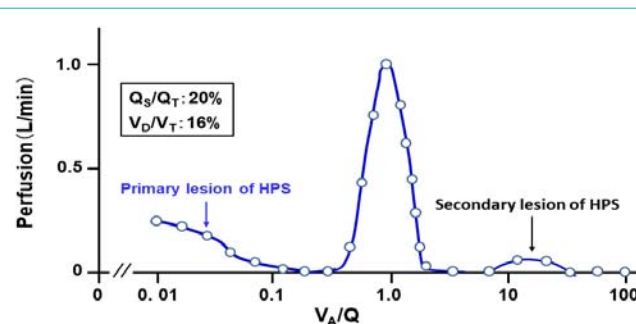

Figure 9: Continuous distribution of V_A/Q in patient with HPS.
MIGET was performed under condition at inspired O_2 concentration of 28%. Acini with right-to-left shunt and low V_A/Q values are primarily formed by those having dilated microvessels with HPV paralysis. Acini with high V_A/Q values are secondarily formed by shift of perfusion from normal acini to those with abnormal microvessels with HPV paralysis.

the communications locating at respiratory bronchioles or alveolar ducts, may further promote the homogenization of spatial gas difference in the acinus. Thus, joining together the result for the functional (imaginary) boundary between dead space and alveolar gas exchange region argued above and the result found by Swan and Tawhai [23], we can infer that the anatomically-defined acinus of HB serves as the functional gas exchange unit during expiration in a first approximation. However, we should be aware of the fact that there is no acinar region rigorously satisfying the definition of the functional gas exchange unit during inspiration. These ideas lead to a critical conclusion that the steady-state gas exchange parameters estimated from the gas samples harvested on expiration can be interpreted based on a concept of the functional gas exchange unit, which implies that the expiration-associated gas exchange parameters, such as the continuous distribution of V_A/Q, reflect the structural abnormalities of bronchioles and microvessels occurring at the acinar level of HB.

Determination of Ventilation-Perfusion (V_A/Q) Distribution in the Lung

There are a couple of important examinations that detect the functional abnormalities occurring at the acinar level, including

the normalized N_2 alveolar plateau estimated from the first few breaths of the Multi-Breath N_2 Washout (MBNW), the Multiple Inert Gas Elimination Technique (MIGET), and so on. Although the normalized N_2 alveolar plateau in the few breaths just after beginning of the MBNW is promising for detecting the Diffusion-Convection-Dependent Inhomogeneity (DCDI) in the acinar regions, which reflects the intra-acinar maldistribution of ventilation [37,46,47], we would like to focus on the MIGET in the present review. This is because the V_A/Q distribution recovered from the MIGET identifies functional abnormalities evoked both by maldistribution of microcirculation and that of alveolar ventilation. The detection of microcirculatory abnormalities is not possible from the MBNW.

Basic rationale for V_A/Q distribution: Under a steady state condition in which there is no change in the Partial Pressure of a gas (P) against the elapsed time (t) at any portion of the lung (i.e., $\partial P/\partial t$ = zero)), the partial pressure of a foreign inert gas in gas phase (P_A) and that in blood phase (P_C) in a given micro region of the lung periphery (compartment) are described by the simple equation in accordance with the law of mass balance [48,49];

$$P_A/P_V = P_C/P_V = \lambda/(\lambda + V_A/Q) \cdots\cdots \text{Equation 2}$$

where P_V denotes the partial pressure of a given inert gas in mixed venous blood, whereas λ is the blood-gas partition coefficient of a gas [50]. The (Equation 2) is valid when an intended gas is not contained in the inspired gas. The (Equation 2) implies that the partial pressure of an inert gas in a microregion of the lung periphery simply decided by the ratio of effective ventilation (V_A) and perfusion (Q) distributed there (Figure 4) [2,51-53]. Although there are many physiological assumptions required for the establishment of (Equation 2) [52-54], they were extensively addressed elsewhere [1,2]. However, the fundamentally important issue that should be emphasized is that the (Equation 2) is implicitly prerequisite for the presence of microregional compartment satisfying the definition of functional gas exchange unit. As extensively argued in the previous section, the microregion given by the acinus of HB encounters the definition of functional gas exchange unit in expiration (Figure 3). However, one should be careful about the fact that the acinus of HB does not satisfy the definition of functional gas exchange unit in inspiration. Fortunately, the MIGET measures inert gas concentrations collected only in expiration so that the V_A/Q distribution investigated from this method can be interpreted based on the concept of functional gas exchange unit, which corresponds to the anatomically-defined microregion really existing in the lung periphery.

Determination of continuous distribution of V_A/Q by MIGET: Saline containing a small quantity of six foreign inert gases with a wide variety of λ, including Sulfur Hexafluoride (SF_6), ethane, cyclopropane, halothane, diethyl ether, and acetone (Table 2), is infused through the peripheral vein at a constant rate of 2 mL/min [52,54]. After a steady state is established (about 30 min after starting the infusion), expired gas, arterial blood, and mixed venous blood are simultaneously collected and the concentrations of six inert gases in these samples are measured by gas chromatography [55]. Using the data measured for six inert gases, Wagner and colleagues [52-54] established a novel method allowing for predicting a continuous distribution of V_A/Q in a representative manner. In this method, they assumed 50 functional gas exchange units with different V_A/Q values,

Figure 10: CT image in patient with intravascular lymphomatosis (IVL). Red circle: thickened lobular septum in association with micronodules and ground glass opacity in left lung field but there are no abnormal shadows in other fields.
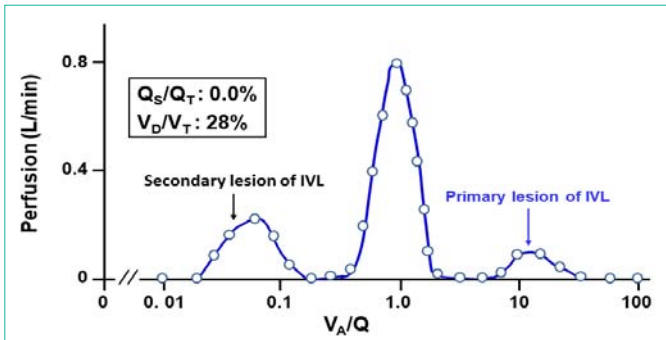

Figure 11: Continuous distribution of V_A/Q in patient with IVL. Acini with high V_A/Q values are primarily yielded by microvascular occlusion with intravascular invasion of B-cell lymphoma cells. Acini with low V_A/Q values are secondarily yielded by shift of perfusion from abnormal acini having microvascular occlusion without HPV paralysis to normal acini.

including right-to-left shunt with V_A/Q of zero, dead space with infinite V_A/Q composed of series (common) and parallel (alveolar) dead space, and 48 units with finite values of V_A/Q ranging from 0.005 to 100, all of which are arranged in parallel and are equally spaced on a logarithmic scale (Figure 5). The basic equation used for determining the continuous distribution of fractional Q (q) along the V_A/Q axis is described below [52-54,56];

$$L = \Sigma W_i[R_i - \Sigma q_j.(\lambda_i/(\lambda_i + (V_A/Q)_j))]^2 + \mu.(1 - \Sigma q_j) + S.\Sigma \phi_j q_j^2$$
$$\cdots\cdots\cdots\text{Equation 3}$$

where L is the objective variable that should be minimized with respect to the fractional perfusion (q_j, j=1, 2 ... 50) distributed to each functional gas exchange unit with a certain V_A/Q value. R_i is the measured value of arterial gas concentration for each inert gas divided by its mixed venous concentration (i=1, 2, … 6). W_i is the coefficient for weight of each inert gas, which is given by the reciprocal of variance of R_i. The second term of the equation denotes the equality constrain for q_j, the sum of which should amount to 1.0. μ is the Lagrange multiplier that is determined and replaced by an adequate value during computation. The third term designates the correction based on the enforced smoothing using the Lagrange multiplier of ϕ_j, which is the value related to the compartmental weight of each V_A/Q unit, while S is the smoothing term that is empirically assumed to be 40. The enforced smoothing is applied for stabilizing the resultant

Table 3: Pathological causes for forming low and high V_A/Q acini.

Low V_A/Q acini	High V_A/Q acini
Primary lesions	**Primary lesions**
1) Destruction or obstruction of acinar airways	1) Microvascular loss
. Acinar Bronchiolitis (COPD) . Atelectasis/pneumonia . Interstitial Pneumonia (IP) . Alveolar edema (ARDS, heart failure, Pulmonary Alveolar Proteinosis (PAP)) . Alveolar Hemorrhage/Infarction (ANCA-related angiitis, Goodpasture, PE)	. COPD . Interstitial Pneumonia (IP) . Pulmonary Embolism (PE) . Cystic disease . Langerhans Cell Histiocytosis (LCH) . Lymphangioleiomyomatosis (LAM)
2) Microvascular injury with HPV paralysis . Hepatopulmonary Syndrome (HPS) . ARDS . Pneumonia (pneumococcus, pseudomonas) . Granulomatous disease . Lung cancer	2) Microvascular occlusion without HPV paralysis . Intravascular Lymphomatosis (IVL) . Pulmonary Veno-Occlusive Disease (PVOD) . Pulmonary Capillary Hemangiomatosis (PCH)
3) Aqueous-phase diffusion limitation (shunt) . HPS, ARDS	
Secondary lesions	**Secondary lesions**
1) Shift of perfusion from acini with microvascular loss or microvascular occlusion without HPV paralysis to normal acini . COPD, IP, PE, LCH, LAM . IVL, PVOD, PCH	1) Shift of ventilation from affected acini to normal acini . Bronchiolitis Obliterans (BO) . Emphysema/bulla (COPD) . Cystic disease (LCH, LAM) . Pleuroparenchymal Fibroelastosis (PPFE)
	2) Shift of perfusion from normal acini to those with microvascular injury with HPV paralysis . HPS, ARDS

V_A/Q distribution. Replacing q_j in the (Equation 3) by fractional ventilation (v_j), the ventilation distribution along the V_A/Q axis is readily decided, as well.

New Method for Quantitating V_A/Q Distribution: The basic concept on proton Magnetic Resonance Imaging (MRI) for measuring V_A/Q distribution was first proposed about six years ago [57]. This technique combines Arterial Spin Labeling (ASL) measures of regional pulmonary blood flow [58] with oxygen enhanced measures of regional specific ventilation [59] and fast gradient echo measures of regional proton density [60,61] to quantify the regional distribution of V_A/Q ratios. Although the spatial resolution of the V_A/Q image examined by the original proton MRI method was not enough, it has been improved considerably by applying a high-precision MRI such as a 1.5 Tesla system. Using the high-performance proton MRI, Sá et al. [62] measured the regional V_A/Q distribution along the 15-mm sagittal slice located in the mid-clavicular line of the right lung in normal adults. The slice measures approximately 8% of the total lung volume and about 20 min is necessary for completing one examination. The collected image matrix size is 256 x 256, giving the voxel size of 0.04 cm³ and the spatial resolution of 1.0 cm³, the latter of which corresponds to the volume composed of 5~6 acini (Table 1). Sá et al. [62] demonstrated that in normal subjects with no lung diseases, the V_A/Q distribution recovered from the proton MRI method does not differ largely from that measured with the classical MIGET. However, there are several disadvantages in the proton MRI method. This method acquires the data from the lung region corresponding to 8% of the entire lung. Although in normal subjects, the V_A/Q distribution in the lung can be considered relatively uniform so that the V_A/Q distribution estimated from the 8% lung region may approximately represent the overall V_A/Q distribution, this assumption is not allowed for the patients with lung diseases, in whom the V_A/Q distribution in a certain region differs substantially from

other regions. When attempting to measure the V_A/Q distribution in the whole lung in terms of the proton MRI method, it may require about four hours for a single observation, which is too long as the clinical examination. Furthermore, from several technical reasons, it is difficult to measure the region with very low V_A/Q (i.e., the shunt) and that with very high V_A/Q (i.e., the dead space) in terms of the proton MRI method [62]. Based on these facts, we consider that at present, the newly-developed proton MRI method does not outweigh the classical MIGET as the examination in a clinical situation.

V_A/Q Distributions in Patients with Pathologically- and/or Radiologically-confirmed Lung Diseases

According to the concept of the functional gas exchange unit expanded in the previous sections, we can conclude that the V_A/Q distribution harvested from the MIGET reflects the inter-regional heterogeneity of V_A/Q distribution at the acinar level. The basic rationale for the clinical interpretation of V_A/Q heterogeneity is summarized in (Table 3). The lesions forming abnormal acini with low V_A/Q values are primarily yielded by obstruction and/or destruction of acinar airways as well as microvascular injury accompanied by paralysis of Hypoxic Pulmonary Vasoconstriction (HPV). The HPV is the major mechanism for matching between perfusion and ventilation, thus preventing the progressive formation of low V_A/Q acini [63-66]. However, if the HPV is paralytic in injured microvasculature, the perfusion there is not decreased so that the formation of low V_A/Q acini advances. The HPV paralysis was identified in some specific lung diseases, including Hepatopulmonary Syndrome (HPS), Acute Respiratory Syndrome (ARDS), pneumonias, granulomatous disease, and some types of lung cancer [63,66-75]. On the other side, the HPV paralysis was not certified in patients with bronchial asthma, Chronic Obstructive Pulmonary Disease (COPD), Idiopathic Pulmonary Fibrosis (IPF), and Pulmonary Embolism (PE)

Table 4: Pulmonary Function Tests (PFT) in three cases.

PFT parameters	BO	HPS	IVL
VC (L)	2.6	3.0	3.2
FVC (L)	2.2	3.0	3.2
FEV_1 (L)	0.8	2.7	2.4
FEV_1/FVC (%)	36	91	75
ATI (%)	15.4	0.4	0.6
PEF (L/sec)	2.2	8.9	7.0
FEF_{50} (L/sec)	0.3	5.1	3.8
TLC (L)	3.9	not determined	not determined
RV (L)	1.3	not determined	not determined
RV/TLC (%)	35	not determined	not determined
PaO_2 (mmHg)	72	56*	56
$PaCO_2$ (mmHg)	58	36*	35
$AaDO_2$ (mmHg)	7.1	101*	49
D_{LCO} (mL/min/mmHg)	27.8	9.7	10.0
K_{CO} (mL/min/mmHg/L)	5.8	1.9	2.6

*: values are measured at inspired O_2 concentration of 28%.

[76-81].

Since microvessels in HPS are largely dilated, the thickness of plasma layer is considerably increased, leading to the augmented aqueous-phase diffusion limitation (shunt) that causes formation of low V_A/Q acini. In ARDS, airspaces are flooded by edematous fluid, which yields aqueous-phase diffusion limitation, as well [56].

The secondary cause for producing low V_A/Q acini is the redistribution of perfusion from affected to non-affected regions. This phenomenon is recognized in patients with microvascular loss or microvascular occlusion without HPV paralysis, who have the acini with high V_A/Q values (primary lesion) in concomitance with those with low V_A/Q values (secondary lesion).

The microvascular loss or microvascular occlusion without HPV paralysis primarily produces the acini with high V_A/Q values because of reduction in acinar perfusion there.

The secondary cause for forming high V_A/Q acini is the redistribution of ventilation from affected to non-affected regions. This is observed in patients with Bronchiolitis Obliterans (BO), COPD, cystic disease, or Pleuroparenchymal Fibroelastosis (PPFE). The reduction (redistribution) of ventilation at embolized regions in severe Pulmonary Embolism (PE) is sometimes attributed to the hypocapnia-elicited bronchoconstriction [82,83]. However, we cannot agree with this opinion, because CO_2-sentive bronchial smooth muscles are predominantly located along central airways but neither peripheral nor acinar airways, indicating that the hypocapnia-related shift of ventilation, if any, occurs far away from the acinar region, thus lacking in an ability for precisely adjusting the distribution of acinar ventilation. Instead, we think that the reduction in ventilation at embolized regions of PE may be explained from the atelectasis, hemorrhage, and/or infarction formed there. This aspect of PE should be taken as a kind of the primary, but not secondary, cause (Table 3).

In a patient with microvascular injury with HPV paralysis, the perfusion in normal acini may be redistributed to the acini with HPV-paralytic microvascular lesions, thus converting the acini with normal V_A/Q values to those with relatively high V_A/Q values.

To address the considerations as described above in a more practical fashion, we presented the continuous V_A/Q distributions in three cases with pathologically- and radiologically-confirmed lung diseases with specific lesions.

Bronchiolitis Obliteration (BO): The case is a 21-year-old, non-smoking woman, who underwent the allogeneic Hematopoietic Stem Cell Transplantation (HSCT) against the chronic myeloid leukemia. After HSCT, she was progressively conscious of Difficulty in Breathing on Exertion (DOE). She died one year after HSCT. The CT examination confirmed the mosaic perfusion in the right lung field at the level of secondary lobule of Miller (Figure 6). Although the ventilation and perfusion scans revealed large reduction in both ventilation and perfusion in the lower lung fields, the mismatch between the two distributions were not evident (Figure 6). The postmortem autopsy identified the remarkable constriction of membranous bronchioles, including lobular and terminal bronchioles, whereas the acinar structures, including acinar airways, alveolar septa, and microcirculation, were spared. These pathological findings are in accordance with the diagnosis of HSCT-induced BO.

The Pulmonary Function Test (PFT) performed three months after HSCT revealed severe airflow obstruction associated with marked reduction in FEV_1/FVC in associated with increased Air Trapping (ATI) and hyperinflation represented by increased Residual Volume (RV) and RV/TLC (Table 4). PaO_2 was reduced and $PaCO_2$ was elevated whereas Alveolar-Arterial PO_2 Difference ($AaDO_2$) was maintained in normal range. Hemoglobin (Hb)-corrected Diffusing Capacity for Carbon Monoxide (D_{LCO}) and Krogh Factor for CO (K_{CO}) were not impaired.

The V_A/Q analysis made by the MIGET showed the bimodal distribution of V_A/Q with a peak at high V_A/Q acini accompanied by slight increase in dead space ventilation (V_D/V_T) but only 0.1% of right-to-left shunt (Q_S/Q_T) (Figure 7). The high V_A/Q acini and increased V_D/V_T are ascribed to the shift of ventilation from acini having obstructed membranous bronchioles to normal acini (the secondary lesion). The elevated $PaCO_2$ is caused by high V_A/Q acini and increased V_D/V_T, which is defined as alveolar hypoventilation, eliciting hypoxemia but normal $AaDO_2$ in association with elevated $PaCO_2$.

Hepatopulmonary Syndrome (HPS): The case is a 72-year-old, ex-smoking man (life-long cigarette consumption: 20 pack-years), who was observed for the alcohol-elicited liver cirrhosis for a long time. He noticed the DOE during these three years and showed severe hypoxemia (PaO_2: 43 mmHg) under resting condition at air breathing. Although continuous oxygen therapy (O_2 flow: 3L/min) was initiated, the improvement of his subjective symptoms and hypoxemia was limited. Therefore, he was hospitalized to enforce a lung biopsy under Video-Assisted Thoracoscopy (VATS) for definite diagnosis of his lung disease. The perfusion scan using ^{99m}Tc-MAA exhibited 28% shunt from pulmonary circulation to systemic circulation (Figure 8). The biopsy implemented at the left lower lung field revealed a remarkable dilatation and distortion of pulmonary microvessels, including capillaries. Although the patient had no symptoms and

inspection findings consistent with bronchial asthma, he exhibited very high fractional concentration of exhaled nitric oxide (FeNO: 84 ppb), which is suggestive of the enhanced expression of various NO syntheses in the lung of this patient [84-86]. Thus, the patient was diagnosed as suffering from the HPS.

The PFT showed that all spirometric parameters are kept in normal ranges (Table 4). However, severe hypoxemia accompanied by widened $AaDO_2$ with no elevation of $PaCO_2$ was investigated under inspired O_2 concentration of 28%. 100% O_2 breathing increased PaO_2 to 75 mmHg under sitting position but increased it up to 278 mmHg under supine position, indicating the remarkable orthodeoxia. The right-to-left shunt estimated from 100% O_2 breathing was 28.4% in sitting position and 20.7% in supine position, the values being qualitatively consistent with those observed in the perfusion scan. Hb-corrected D_{LCO} and K_{CO} were conspicuously decreased.

The V_A/Q distribution recovered from the MIGET exhibited the trimodal V_A/Q peaks with acini having very low V_A/Q values and augmented shunt as well as those having high V_A/Q values (Figure 9). The acini with very low V_A/Q values and shunt are the primary lesion in the HPS, where microvascular HPV is impaired [74,75]. On the other hand, the acini with high V_A/Q values are produced as the secondary lesion, in which the perfusion in normal acini is shifted to abnormal acini with HPV-paralytic injured microvessels.

Intravascular Lymphomatosis (IVL): The case is a 67-year-old, never-smoking man, who complained of sustained low-graded fever, progressively worsening productive cough, and DOE during a couple of preceding months. The CT examination identified the thickened lobular septum surrounded by micronodules and Ground Glass Opacity (GGO) only in a small part of the left lung but there were no abnormal shadows in other parts (Figure 10). The micronodules may be the shadows yielded by occluded microvessels, while GGO is suggestive of hemorrhage from these abnormal microvessels. The lung tissue sample obtained by the VATS exhibited the marked invasion of B-cell lymphoma cells into the arterioles, venules and capillaries but no invasion outside the microvessels. The microvascular lumens were occluded by the tumor cells. Thus, he was diagnosed as having the IVL, in which the lesion was confined within microvessels while acinar airways and alveolar sleeves were not involved.

The PFT showed normal spirometry, widened $AaDO_2$ and marked reduction in Hb-corrected D_{LCO} and K_{CO} (Table 4).

The MIGET analysis exhibited the trimodal V_A/Q heterogeneity with both low and high V_A/Q acini (Figure 11). The occluded microvessels (without HPV paralysis) primarily yield high V_A/Q acini, while the shift of perfusion from occluded microvessels to normal microvessels generates low V_A/Q acini.

Conclusion

The spatial distribution of PO_2 in the acinus of Haefeli-Bleuer is almost homogeneous over expiration but not over inspiration, leading to the conclusion that the anatomically-defined acinus of Haefeli-Bleuer acts as the functional gas exchange unit in expiration but not in inspiration. As the multiple inert gas elimination technique measures the V_A/Q distribution by analyzing respective concentrations of six inert gases collected over expiration, the V_A/Q heterogeneity thus

determined predicts the mismatch between ventilation and perfusion elicited by abnormal microstructures of airways and/or vessels at the acinar level. The present review certainly indicates that the continuous distribution of V_A/Q estimated by the multiple inert gas elimination technique admits of predicting the microstructural abnormalities at the acinar level, the precious detection of which is very difficult even when a high-resolution CT technology is applied.

References

1. Yamaguchi K, Tsuji T, Aoshiba K, Nakamura H, Abe S. Anatomical backgrounds on gas exchange parameters in the lung. World J Respirol. 2019; 9: 8-28.

2. Wagner PD, West JB. Ventilation-Perfusion Relationships. Pulmonary Gas Exchange. New York: Academic Press. 1980; 219-262.

3. Weibel ER. Principles and methods for the morphometric study of the lung and other organs. Lab Invest. 1963; 12: 131-155.

4. Weibel ER, Crystal RG, West JB, Barnes PJ. Design of Airways and Blood Vessels Considered as Branching Trees. The LUNG Scientific Foundations. Philadelphia: Lippincott-Raven. 1997; 1061-1071.

5. Hsia CCW, Hyde DM, Weibel ER. Lung structure and the intrinsic challenges of gas exchange. Compr Physiol. 2016; 6: 827-895.

6. Piiper J, Scheid P, Fishman AP, Farhi LE, Tenney SM, Geiger SR. Diffusion and Convection in Intrapulmonary Gas Mixing. editors. In: Handbook of Physiology, Section 3: The Respiratory System, Volume IV: Gas Exchange. Bethesda Maryland: American Physiological Society. 1987; 51-69.

7. Haefeli-Bleuer, Weibel ER. Morphometry of the human pulmonary acinus. Anat Rec. 1988; 220: 401-414.

8. Martin H. Respiratory bronchioles as the pathway for collateral ventilation. J Appl Physiol 1966; 21: 1443-1447.

9. Sobin SS, Fung YC, Lindal RG, Tremer HM, Clark L. Topology of pulmonary arterioles, capillaries, and venules in the cat. Microvasc Res 1980; 19: 217-233.

10. Webb WR, Müller NL, Naidich DP. Illustrated Glossy of High-Resolution Computed Tomography. Webb WR, Müller NL, Naidich DP, editors. In: High-Resolution CT of the Lung. 3rd edn. Philadelphia: Lippincott Williams & Wilkins. 2001; 599-618.

11. Engel S. Lung Structure. Illinois: Springfield. 1962.

12. Pump KK. Morphology of the acinus of the human lung. Dis Chest. 1969; 56: 126-134.

13. Boyden EA. The structure of the pulmonary acinus in a child of six years and eight months. Am J Anat. 1971; 132: 275-299.

14. Parker H, Horsfield K, Cumming G. Morphology of distal airways in the human lung. J Appl Physiol. 1971; 31: 386-391.

15. Hansen JE, Ampaya EP. Human air space shapes, sizes, areas, and volumes. J Appl Physiol. 1975; 38: 990-995.

16. Schreider JP, Raabe OG. Structure of the human respiratory acinus. Am J Anat. 1981; 162: 221-232.

17. Miller WS. The Lung. Illinois: Springfield. 1947; 162-204.

18. Itoh H, Murata K, Konishi J. Diffuse lung disease: pathologic basis for the high-resolution computed tomography findings. J Thorac Imag. 1993; 8: 176-188.

19. Reid L, Simon G. The peripheral pattern in the normal bronchogram and its relation to peripheral pulmonary anatomy. Thorax. 1958; 13: 103-109.

20. Reid L. The secondary lobule in the adult human lung, with special reference to its appearance in bronchograms. Thorax. 1958; 13: 110-115.

21. Aschoff L. Lectures on Pathology. New York: Hoeber, 1924; 53-57.

22. König MF, Lucocq JM, Weibel ER. Determination of pulmonary vascular perfusion by electron and light microscopy. J Appl Physiol. 1993; 75: 1877-

1883.

23. Swan AJ, Tawhai MH. Evidence for minimal oxygen heterogeneity in the healthy human pulmonary acinus. J Appl Physiol. 2011; 110: 528-537.

24. Schreider JP, Hutchens JO. Morphology of the guinea pig respiratory tract. Anat Rec. 1980; 196: 313-321.

25. Mitzner W, Crystal RG, West JB, Weibel ER, Barnes PJ. Collateral Ventilation. The LUNG Scientific Foundations. Philadelphia: Lippincott-Raven. 1997; 1425-1435.

26. Lambert MW. Accessory bronchiole-alveolar communications. J Pathol Bacteriol. 1955; 70: 311-314.

27. Duguid JB, Lambert MW. The pathogenesis of coal miner's pneumoconiosis. J Pathol Bacteriol. 1964; 88: 389-403.

28. Raskin SP, Herman PG. Interacinar pathways in the human lung. Am Rev Respir Dis. 1975; 111: 489-495.

29. Anthonisen NR, Fleetham JA, Fishman AP, Farhi LE, Tenney SM, Geiger SR. Ventilation: Total, Alveolar, and Dead Space. Handbook of Physiology, Section 3: The Respiratory System, Volume IV: Gas Exchange. Bethesda Maryland: American Physiological Society. 1987; 113-129.

30. Loewy A. Uber die Bestimmung der Grosse des "Sehadlichen Luftraumes" im thorax und der alveolaren Sauersttoffs-panung. Arch Gesamte Physiol Menschen Tiere. 1894; 58: 416-427.

31. Rohrer F. Der Strömmungswiderstand in den menschlichen Atemwegen und Einffluss der unregelmässigen Verzweigung des Bronchialsystems auf den Atmungsverlauf in verschiedenen Lungenberizieken. Pfluegers Arch Gesamte Physiol Menschen Tiere. 1915; 162: 225-299.

32. Nunn JF, Campbell EJM, Peckett BW. Anatomical subdivisions of the volume of respiratory dead space and effect of position of the jaw. J Appl Physiol. 1959; 14: 174-176.

33. Fowler WS. Lung Function studies. II. The respiratory dead space in old age and in in pulmonary emphysema. J Clin Invest. 1950; 28: 1439-1444.

34. Bartels J, Severinghaus JW, Forster RE, Briscoe WA, Bates DV. The respiratory dead space measured by single breath analysis of oxygen, carbon dioxide, nitrogen or helium. J Clin Invest. 1954; 33: 41-48.

35. Young AC. Dead space at rest and during exercise. J Appl Physiol. 1955; 50: 91-94.

36. Lacquet LM, Van Der Linden, Paiva M. Transport of H2 and SF6 in the lung. Respir Physiol. 1975; 25: 157-173.

37. Verbanck S, Paiva M. Gas mixing in the airways and airspaces. Compr Physiol. 2011; 1: 809-834.

38. Gomez DM. A physico-mathematical study of lung function in normal subjects and in patients with obstructive pulmonary diseases. Med Thorac. 1965; 22: 275-294.

39. Paiva M. Gas transport in the human lung. J Appl Physiol. 1973; 43: 401-410.

40. Weibel ER. Morphometry of the human lung. Berlin: Springer-Verlag. 1963.

41. Phalen RF, Yeh HC, Schum GM, Raabe OG. Application of an idealized model to morphometry of the mammalian tracheobronchial tree. Anat Rec. 1978; 190: 167-176.

42. Phalen RF, Oldham MJ, Beaucage CB, Crocker TT, Mortensen JD. Postnatal enlargement of human tracheobronchial airways and implications for particle deposition. Anat Rec. 1985; 212: 368-380.

43. Yeh HC, Schum GM. Models of human lung airways and their application to inhaled particle deposition. Bull Math Biol. 1980; 42: 461-480.

44. La Force RC, Lewis BM. Diffusional transport in the human lung. J Appl Physiol. 1970; 28: 291-298.

45. Paiva M. Two new pulmonary functional indexes suggested by a simple mathematical model. Respiration. 1975; 32: 389-403.

46. Paiva M, Engle LA. The anatomical basis for the sloping N_2 plateau. Respir Physiol. 1981; 44: 325-337.

47. Crawford AB, Makowska M, Paiva M, Engel LA. Convection- and diffusion-dependent ventilation maldistribution in normal subjects. J Appl Physiol. 1985; 59:838-846.

48. Kety S. The theory and applications of the exchange of inert gas at the lungs and tissues. Pharmacol Rev. 1951; 3: 1-41.

49. Farhi LE. Elimination of inert gas by the lung. Respir Physiol. 1967; 3: 1-11.

50. Piiper J, Dejours P, Haab P, Rahn H. Concepts and basic quantities in gas exchange physiology. Respir Physiol. 1971; 13: 294-304.

51. Yokoyama T, Farhi LE. Study of ventilation-perfusion ratio distribution in the anesthetized dog by multiple inert gas washout. Respir Physiol. 1967; 3: 166-176.

52. Wagner PD, Saltzman H, West JB. Measurement of continuous distributions of ventilation-perfusion ratios: Theory. J Appl Physiol. 1974; 36: 588-599.

53. West JB, Wagner PD, Crystal RG, West JB, Weibel ER, Barnes PJ. Ventilation-Perfusion Relationships. The LUNG Scientific Foundations. Philadelphia: Lippincott-Raven Publishers. 1997: 1693-1709.

54. Wagner PD, Laravuso RB, Uhl RR, West JB. Continuous distributions of ventilation-perfusion ratios in normal subjects breathing air and 100% O_2. J Clin Invest 1974; 54: 54-68.

55. Wagner PD, Naumann PF, Laravuso RB. Simultaneous measurement of eight foreign gases in blood by gas chromatography. J Appl Physiol. 1974; 36: 600-605.

56. Yamaguchi K, Mori M, Kawai A, Takasugi T, Asano K, Oyamada Y, et al. Ventilation-perfusion inequality and diffusion impairment in acutely injured lungs. Respir Physiol. 1994; 98: 165-177.

57. Henderson AC, Sá RC, Theilmann RJ, Buxton RB, Prisk GK, Hopkins SR. The gravitational distribution of ventilation-perfusion ratio is more uniform in prone than supine posture in the normal human lung. J Appl Physiol. 2013; 115: 313-324.

58. Burnham KJ, Arai TJ, Dubowitz DJ, Henderson AC, Holverda S, Buxton RB, et al. Pulmonary perfusion heterogeneity is increased by sustained, heavy exercise in humans. J Appl Physiol. 2009; 107: 1559-1568.

59. Sá RC, Cronin MV, Henderson AC, Holverda S, Theilmann RJ, Arai TJ, et al. Vertical distribution of specific ventilation in normal supine humans measured by oxygen-enhanced proton MRI. J Appl Physiol. 2010; 109: 1950-1959.

60. Theilmann RJ, Arai TJ, Samiee A, Dubowitz DJ, Hopkins SR, Buxton RB, et al. Quantitative MRI measurement of lung density must account for the change in T(2) (*) with lung inflation. J Magn Reason Imaging. 2009; 30: 527-534.

61. Holverda S, Theilmann RJ, Sá RC, Arai TJ, Hall ET, Dubowitz DJ, et al. Measuring lung water: ex vivo validation of multi-image gradient echo MRI. J Magn Reson Imaging. 2011; 34: 220-224.

62. Sá RC, Henderson AC, Simonson T, Arai TJ, Wagner H, Theilmann RJ, et al. Measurement of the distribution of ventilation-perfusion ratios in the human lung with proton MRI: comparison with the multiple inert-gas elimination technique. J Appl Physiol. 2017; 123: 136-146.

63. Yamaguchi K, Suzuki K, Nishio K, Aoki T, Suzuki Y, Miyata A, et al. Biological Impediment to Oxygen Sensing in Injured Pulmonary Microcirculation Exposed to High Oxygen Environment. Ishimura Y, Shimada H, Suematsu M, editors. In: Oxygen Homeostasis and Its Dynamics. Tokyo: Springer-Verlag. 1997; 410-420.

64. Yamaguchi K, Mori M, Kawai A, Takasugi T, Oyamada Y, Koda E. Inhomogeneities of ventilation and of the diffusing capacity to perfusion ratio in various chronic lung diseases. Am J Respir Crit Care Med. 1997; 156: 86-93.

65. Yamaguchi K, Suzuki K, Naoki K, Nishio K, Sato N, Kudo H, et al. Response of intraacinar pulmonary microvessels to hypoxia, hypercapnic acidosis and isocapnic acidosis. Circ Res. 1999; 82: 722-728.

66. Naoki K, Yamaguchi K, Suzuki K, Kudo H, Nishio K, Sato N, et al. Nitric oxide differentially attenuates microvessel response to hypoxia and hypercapnia in injured lungs. Am J Physiol (Regulatory, Integrative and Comparative

Physiology). 1999; 277: 181-189.

67. Hales CA, Sonne L, Peterson M, Kong D, Miller M, Watkins, et al. Role of thromboxane and prostacyclin in pulmonary vasomotor changes after endotoxin in dogs. J Clin Invest. 1981; 68: 497-505.

68. Hutchison AA, Ogletree ML, Snapper JR, Brigham KL. Effect of endotoxemia on hypoxic pulmonary vasoconstriction in unanesthetized sheep. J Appl Physiol. 1985; 58: 1463-1468.

69. Leeman M, Delcroix M, Vachiéry JL, Mélot C, Naeije R. Blunted hypoxic vasoconstriction in oleic acid lung injury: effect of cyclooxygenase inhibitors. J Appl Physiol. 1992; 72: 251-258.

70. Light RB. Indomethacin and acetylsalicylic acid reduce intrapulmonary shunt in experimental pneumococcal pneumonia. Am Rev Respir Dis. 1986; 134: 520-525.

71. Graham LM, Vasil A, Vasil ML, Voelkel NF, Stenmark KR. Decreased pulmonary vasoreactivity in an animal model of chronic Pseudomonas pneumonia. Am Rev Respir Dis. 1990; 142:221-229.

72. Irwin RS, Martinez-Gonzalez-Rio J, Thomas HM 3rd, Fritts HW. The effect of granulomatous pulmonary disease in dogs on the response of the pulmonary circulation to hypoxia. J Clin Invest. 1977; 60: 1258-1265.

73. Schulman LL, Wood JA, Enson Y. Control of shunt pathway perfusion in diffuse granulomatous lung disease. J Appl Pysiol. 1989; 67 :1717-1726.

74. Hoeper MM, Krowka MJ, Strassburg CP. Portopulmonary hypertension and hepatopulmonary syndrome. Lancet. 2004; 363:1461-1468.

75. Rodríguez-Roisin R, Krowka MJ. Hepatopulmonary syndrome - a liver-induced lung vascular disorder. N Engl J Med. 2008; 358: 2378-2387.

76. Rodriguez-Roisin R, Ballester E, Roca J, Torres A, Wagner PD. Mechanisms of hypoxemia in patients with status asthmaticus requiring mechanical ventilation. Am Rev Respir Dis. 1989; 139: 732-739.

77. Ballester E, Roca J, Ramis L, Wagner PD, Rodriguez-Roisin R. Pulmonary gas exchange in severe chronic asthma. Response to 100% oxygen and salbutamol. Am Rev Respir Dis. 1990; 141: 558-562.

78. Agustí AG, Barberá JA, Roca J, Wagner PD, Guitart R, Rodriguez-Roisín R. Hypoxic pulmonary vasoconstriction and gas exchange during exercise in chronic obstructive pulmonary disease. Chest. 1990; 97: 268-275.

79. Barberà JA, Riverola A, Roca J, Ramirez J, Wagner PD, Ros D, et al. Pulmonary vascular abnormalities and ventilation-perfusion relationships in mild chronic obstructive pulmonary disease. Am J Respir Crit Care Med. 1994; 149: 423-429.

80. Agustí AG, Roca J, Gea J, Wagner PD, Xaubet A, Rodriguez-Roisin R. Mechanisms of gas-exchange impairment in idiopathic pulmonary fibrosis. Am Rev Respir Dis. 1991; 143: 219-225.

81. Burrowes KS, Clark AR, Wilsher ML, Milne DG, Tawhai MH. Hypoxic pulmonary vasoconstriction as a contributor to response in acute pulmonary embolism. Ann Biomed Eng. 2014; 42: 1631-1643.

82. Giuntini C. Ventilation/perfusion scan and dead space in pulmonary embolism: are they useful for the diagnosis? Q J Nucl Med. 2001; 45: 281-286.

83. Ferreira JH, Terzi RG, Paschoal IA, Silva WA, Moraes AC, Moreira MM. Mechanisms underlying gas exchange alterations in an experimental model of pulmonary embolism. Braz J Med Biol Res. 2006; 39: 1197-1204.

84. Cremona G, Higenbottam TW, Mayoral V, Alexander G, Demoncheaux E, Borland C, et al. Elevated exhaled nitric oxide in patients with hepatopulmonary syndrome. Eur Respir J. 1995; 8: 1883-1885.

85. Delclaux C, Mahut B, Zerah-Lancner F. Increased nitric oxide output from alveolar origin during liver cirrhosis versus bronchial source during asthma. Am J Respir Crit Care Med. 2002; 165: 332-337.

86. Rolla G, Brussino L, Scappaticci E. Source of exhaled nitric oxide in primary biliary cirrhosis. Chest. 2004; 126: 1546-1551.